Available online at www.sciencedirect.com

ScienceDirect

Energy Procedia 35 (2013) 43 – 51

Energy Procedia

DeepWind'2013, 24-25 January, Trondheim, Norway

Towards the fully-coupled numerical modelling of floating wind turbines

Axelle Viré[a*], Jiansheng Xiang[a], Matthew Piggott[a,b], Colin Cotter[c], Christopher Pain[a]

[a]*Department of Earth Science and Engineering, Imperial College London, South Kensington Campus, SW7 2AZ London, UK*
[b] *Grantham Institute for Climate Change, Imperial College London, South Kensington Campus, SW7 2AZ London, UK*
[c]*Department of Aeronautics, Imperial College London, South Kensington Campus, SW7 2AZ London, UK*

Abstract

The aim of this study is to model the interactions between fluids and solids using fully nonlinear models. Non-linearity is important in the context of floating wind turbines, for example, to model breaking waves impacting on the structure and the effect of the solid's elasticity. The fluid- and solid-dynamics equations are solved using two unstructured finite-element models, which are coupled at every time step. Importantly, the coupling ensures that the action-reaction principle is satisfied at a discrete level, independently of the order of representation of the discrete fields. To the authors' knowledge, the present algorithm is novel in that it can simultaneously handle: (i) non-matching fluid and solid meshes, (ii) different polynomial orders of the basis functions on each mesh, and (iii) different fluid and solid time steps. First, results are shown for the flow past a fixed actuator-disk immersed in a uniform flow and representing a wind turbine. The present numerical results for the velocity deficit induced by the disk are shown to be in good agreement with the semi-analytical solution, for three values of thrust coefficients. The presence of a non-zero fluid viscosity in the numerical simulation affects wake recovery and fluid entrainment around the disk. Second, the dynamic response of a cylindrical pile is computed when placed at an interface between air and water. The results qualitatively demonstrate that the present models are applicable to the modelling of multiple fluids interacting with a floating solid. This work provides a first-step towards the fully coupled simulation of offshore wind turbines supported by a floating spar.

* Corresponding author. Tel.: +44-(0)20-7594-2921.
E-mail address: avire@imperial.ac.uk.

doi:10.1016/j.egypro.2013.07.157

Keywords: Fluid-structure interactions; floating wind turbines; Actuator disk; Unstructured meshes; Finite-element methods; Adaptive remeshing

Nomenclature

C_T	Thrust coefficient of the wind turbine.
D	Diameter of the disk and the pile.
F_f	Action-reaction force exerted by the solid on the fluid.
F_s	Action-reaction force exerted by the fluid on the solid.
μ	Dynamic viscosity of the fluid.
ρ	Density of the fluid.
u	Monolithic velocity field.
u_s	Solid velocity field.

1. Introduction

The numerical modelling of fluid-structure interactions is important in the context of offshore renewable energy devices. This work targets floating wind turbines, where a floating pile moored to the seabed supports the wind turbine [22]. Such devices are suitable in deep seas (typically deeper than 50 metres), where bottom-mounted foundations are too expensive. The dynamic interaction between the moving air-water and fluid-solid interfaces, and the presence of both rigid and deformable solids, render the numerical modelling of floating wind turbines very challenging. Numerical models are attractive in studying such coupled fluid-solid problems, because they can analyse different configurations while limiting expensive laboratory testing. A number of aero-hydro-servo-elastic models exist to analyse the dynamic behaviour of floating wind turbines. Methods to compute the hydrodynamics of the floating structure include: (i) linear radiation-diffraction codes, (ii) inviscid fully-nonlinear models (typically based on a velocity potential formulation), and (iii) viscous fully-nonlinear models (for solving the Navier–Stokes equations). Linear radiation-diffraction codes and potential flow formulations are commonly used in the context of spar-buoy supports, as discussed by Jonkman et al. [6] for seven different models (i.e. FAST, Bladed, ADAMS, HAWC2, 3Dfloat, Simo, and SESAM/DeepC). Additional recent analyses of the wave-induced motions of a spar buoy include Karimirad et al. [7] and Karimirad [8] using the DeepC and HAWC2 models, and Sethuraman [20] using the time-domain finite-element solver OrcaFlex. By contrast with linear and potential-flow approaches, computational fluid dynamics tools based on the solution of the Navier–Stokes equations are particularly appealing for investigating extreme wave conditions. Viscous non-linear models can resolve the effect of fluid viscosity and air entrainment on the system dynamics. However, they often fail to simulate wave propagation over long distances, due to excessive numerical dissipation [10]. Recently, the suitability of Fluidity-ICOM for modelling both wave propagation and wave-structure interactions was demonstrated in two- [21] and three- [24] dimensions. Fluidity-ICOM is an open-source finite-element model, which solves the non-hydrostatic Navier–Stokes equations on unstructured meshes [14, 16]. In terms of modelling the aerodynamics of wind turbines, the simplest approach is to replace the turbine by a thin actuator disk [4], which exerts a uniform thrust force on the flow. Despite its simplicity, the actuator-disk model is often

useful to reproduce wind deficits and wake losses [3]. However, it presents certain limitations such as the absence of swirl and tip vortices induced in the flow. A series of improved actuator-disk models are referenced in the literature [12]. For engineering applications, the aerodynamic forces are commonly computed using blade-element momentum or generalized dynamic wake approaches, with or without dynamic stall, see for example [6, 9]. Sebastian and Lackner [18] highlighted that classical momentum balance approaches are not always adequate for modelling floating wind turbines, due to the aerodynamic unsteadiness associated with the floating support motions. They proposed a free-vortex method tailored for floating wind turbines, based on the assumption of potential flow [19]. Finally, the elastic structural dynamics of floating wind turbines is generally based on multi-body dynamics formulations, quasi-static analyses, or finite-element methods [6].

The use of separate models to simulate mutual interactions between fluids and solids present several advantages. For example, the different spatial and temporal discretisations in each model allows for the resolutions to be tailored to the specific needs of the fluids and solids. Recently, Fluidity-ICOM was coupled to the finite-discrete element (femdem) model Y3D [26], which solves for the non-linear dynamics of solid structures. In this context, solids were represented as immersed in an extended mesh (covering both fluids and solids) and their effect on the fluid dynamics was accounted for as an additional source term in the momentum equations. This methodology underpins the original immersed boundary method, proposed by Peskin [15], and which was further modified as reviewed in the literature; see for example [5, 11, 13]. Viré et al. [23] presented a novel algorithm to ensure spatial conservation of the action-reaction force, when projected between both models. As opposed to other existing techniques, the algorithm enables: (i) arbitrarily high orders of representation of the discrete fields, and (ii) different representations of the discrete fields in each model.

The coupled models Fluidity-ICOM and Y3D could complement existing tools for modelling floating wind turbines over short time intervals, by providing the fully non-linear response of the coupled system under extreme environmental conditions. At this stage, the main purpose is to validate the current computational models on flows of fundamental interests, for which semi-analytical solutions exist. In this paper, the coupled models are applied to the simulation of: (i) a fixed actuator-disk representing a wind turbine, and (ii) a pile of uniform density floating at an air-water interface. The application to more complex turbine models and realistic floating wind turbine supports is the subject of further investigation. The paper is organised as follows. The general principle of the method and the governing equations are derived in Section 2. Section 3 presents the conservative coupling algorithm between the fluid and solid models. Results are shown in Section 4, and conclusions are drawn in Section 5.

2. Mathematical formulation

2.1. Governing equations

Considering a solid V_s immersed in a fluid domain V_f, an extended domain $V=V_f \cup V_s$ can be defined by filling the solid regions with the surrounding fluid. The interactions between fluids and solids in this domain are modelled by relaxing the flow to the behaviour of the solids in the regions $V_f \cap V_s$. On the one hand, the finite-element model Y3D [26] solves the solid-dynamics equations on a solid mesh covering the solid domain V_s. The equations are expressed as

$$\mathcal{L}d_s + F_{int} = F_{ext} + F_c + F_s,$$

where d_s denotes the solid displacement, $\mathcal{L}$ is an operator dependent on the velocity gradient, F_{int} stands for the internal forces, F_c is the contact force when multiple solids impact on each other, and F_{ext} is the

external force including the surface traction force and the body forces. The action-reaction force exerted by the fluid is denoted by F_s. On the other hand, the finite-element model Fluidity-ICOM [14, 16] solves the fluid-dynamics equations on a *fluid mesh* covering the extended domain V. The Navier–Stokes equations are therefore solved for a monolithic velocity $u = \alpha_f u_f + \alpha_s u_s$, where $\alpha_i = V_i/V$ is the volume fraction and the subscript indicates the material (*f* for fluid and *s* for solid). The equations are

$$\nabla \cdot u = 0,$$
$$\rho \frac{\partial u}{\partial t} + \rho(u \cdot \nabla)u = -\nabla p + \nabla(2\mu S) + B + F_f,$$

where ρ is the fluid density, p is the pressure field, μ is the dynamic viscosity of the fluid, S is the deviatoric part of the strain-rate tensor, B represents external body forces (e.g. buoyancy), and F_f is the penalty force that relaxes the monolithic velocity to the solid velocity in V_s. The penalty force is given by

$$F_f = \beta(\alpha_s u_s - \alpha_s u), \tag{1}$$

where $\beta = \rho/\Delta t$ is a factor that dictates how fast the fluid and solid velocities relax to one another at the fluid-structure interface, and Δt is the time step. Periodic re-meshing is performed on the fluid mesh, in order to refine the fluid-structure interface as the solid moves. The discretisation schemes used in each model are reported in Viré et al. [23]. Both models use unstructured finite-element meshes. Time is discretised using a Crank–Nicolson scheme in the fluid-dynamics model and a backward Euler scheme in the solid-dynamics model.

2.2. Coupling between fluid- and solid- dynamics models

The penalty force given by Eq. (1) is exchanged between both models in two distinct steps (Fig. 1). The part of the force depending on the monolithic velocity, i.e. $F_1 = -\beta\alpha_s u$, is exchanged from fluid to solid model, while the part dependent on the solid velocity, i.e. $F_2 = \beta\alpha_s u_s$, is transferred from solid to fluid model. The projection steps are detailed in Viré et al. [23]. The force F_1 is computed on a supermesh, which is formed from the intersections between fluid and solid meshes. This force is projected to the fluid and solid meshes using a Galerkin projection. This ensures that the volume integral of F_1 is identical on each mesh, independently of: (i) the mesh resolutions, and (ii) the polynomial orders of the basis functions on each mesh. Because the solid mesh lies within the fluid mesh, a Galerkin projection of F_2 from solid to fluid mesh satisfies the same conservation property [23]. In order to resolve the propagation of stresses inside non-rigid solids, and because the solid solver is fully explicit in time, the solid time-step is typically smaller than the fluid time-step. Therefore, the force F_2 is averaged over the solid time-steps before being projected to the fluid model.

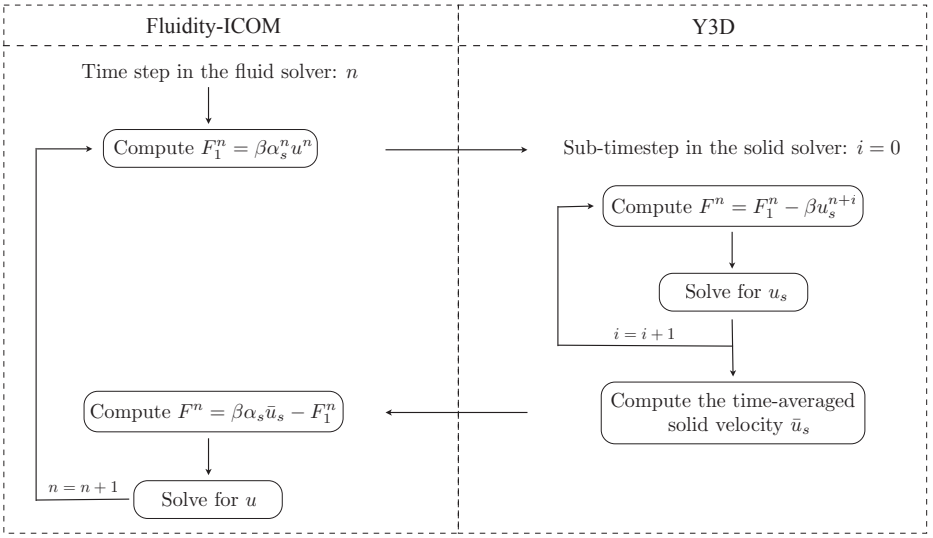

Figure 1: Sketch of the sequence of steps of the coupled models, and their respective time loops.

3. Results

3.1. Uniform flow past a fixed actuator disk

Wind turbines can be parameterised by thin disks, over which a thrust force is uniformly spread. The force acting on the fluid is derived from the actuator-disk theory [4], which assumes that the flow is homogeneous, incompressible, steady, friction-less and that no external force acts on the fluid up- or down-stream of the rotor. The thrust force is given by

$$T = \frac{1}{2}\rho C_T A_d u_0^2,$$

where C_T is the thrust coefficient of the wind turbine, A_d is the disk frontal-area, and u_0 is the far-upstream velocity. The disk area, thrust coefficient, and fluid density, are input parameters of the model. The far-upstream velocity u_0 is calculated by defining an axial-induction factor a as

$$a = 1 - \frac{u_{hub}}{u_0},$$

where u_{hub} is the numerical velocity probed at the disk at every time iteration in the fluid-dynamics model. The axial-induction factor is further related to the thrust coefficient of the turbine [4] by

$$a = \frac{1}{2}\left(1 - \sqrt{1 - C_T}\right).$$

This turbine parameterisation presents certain limitations, including the absence of swirl and tip vortices induced in the flow. Thus, it is unsuitable for computing the aerodynamics of a three-bladed rotor under realistic conditions. However, it is often adopted when modelling farms of wind turbines, see for example [2, 17]. The actuator-disk representation is chosen in this study for two reasons. First, the purpose is to validate the model on flows where a semi-analytical solution exists. Second, there is a rising interest for

modelling farms of tidal turbines using Fluidity-ICOM, in which case coupling an actuator-disk model with a hydrodynamic model for the ocean is important. For validation purposes, fixed turbines are considered. Thus, the solid model does not solve the solid-dynamics equations. However, two meshes are used as described in the previous section: the fluid mesh covers the whole computational domain, while the solid mesh only discretises the disk. A solid-concentration field is defined on the fluid mesh, in order to identify the region occupied by the disk. This field is obtained by projecting a unitary field from solid to fluid mesh using a Galerkin projection. The thrust force acting on the fluid is spread uniformly across the disk. The disk centre is placed at a distance of $20D$ from the domain outlet, and 5D from the inlet and sides (D being the disk diameter). The disk axis is aligned with the flow. The Reynolds number is set to $\mathrm{Re_D} = \rho \mathrm{u_0 D}/\mu = 10^3$, and three values of the thrust coefficients are considered ($C_T = 0.2; 0.45; 0.7$). The fluid model has the capability to optimise the mesh at given intervals in time, in order to refine the resolution around certain flow features. In this work, the fluid mesh is adapted at a non-dimensional period of $\mathrm{T\,u_0/D} = 1$ and refines the regions of high curvatures in the velocity and pressure fields. The mesh therefore tracks the small-scale dynamics developing in the vicinity of the disk and in the wake, while it coarsens elsewhere. The total number of mesh nodes at steady state is in the order of 10^6. The minimum and maximum values of the element-edge length are respectively of the order of $\mathrm{l_e/D} = 0.015$ and $\mathrm{L_e/D} = 0.7$. The time step is such that the Courant number is fixed at 0.3. All the simulations are ran on 32 processing cores. The typical computational times, for running a non-dimensional time of $\mathrm{T\,u_0/D} = 50$, vary from 90 (for small thrust coefficients) to 240 (for large thrust coefficients) hours. Viré et al. [25] further report the changes in solution accuracy and computational cost for various meshes and disk thicknesses. Figure 2 shows the streamwise evolution of the streamwise velocity at the disk centerline $r = 0$ (left) and at $r = D$ (right). Dash lines indicate the numerical results, while the continuous lines represent the semi-analytical solution [4] given by

$$u_x(x,r) = u_0 - \frac{u_{hub}}{4}\left(\frac{x}{\pi\sqrt{rD/2}}Q_{-1/2}(\omega) + \Lambda_0(\beta,k) + 2\right) \quad \text{if } r < D/2, \tag{2}$$

$$u_x(x,r) = u_0 - \frac{u_{hub}}{4}\left(\frac{x}{\pi\sqrt{rD/2}}Q_{-1/2}(\omega) - \Lambda_0(\beta,k)\right) \quad \text{if } r > D/2. \tag{3}$$

In Eqs. (2)-(3), $\Lambda_0(\beta,k)$ denotes the Heuman's Lambda function, $\mathrm{Q}_{-1/2}(\omega)$ is the Legendre function of the second kind, $k = \sqrt{2rD/m_1}$, $\beta = \mathrm{asin}\,(x/\sqrt{m_2})$, $\omega = (x^2 + r^2 + D^2/4)/\mathrm{rD}$, $m_1 = x^2 + (r + D/2)^2$, and $m_2 = x^2 + (r - D/2)^2$. In the near-field, the velocity deficit induced by the disk at the centreline is well predicted by the present algorithm (Fig. 2 left). The discrepancy between numerical and theoretical results grows larger in the far-wake. This is explained by the role of the fluid viscosity in the numerical simulations. No wake recovery is observed in the theoretical results, which are derived under the inviscid approximation. The fluid viscosity also affects the velocity field away from the disk in the radial direction, particularly at large thrust coefficients (Fig. 2 right). The entrainment of surrounding fluid is larger than predicted theoretically. Figure 3 shows the radial evolution of the velocity deficit at two streamwise locations: on the upstream face of the disk plane (Fig. 3 left) and in the disk wake (Fig. 3 right). Note that the functions Λ_0 and $\mathrm{Q}_{-1/2}$ are continuous in the radial direction, upstream and downstream of the disk. Therefore, following Eqs. (2)-(3), the analytical solution for the streamwise velocity is continuous only if $\Lambda_0(r = D/2) = -1$, which is the case solely upstream of the uniformly loaded disk. This explains the discontinuity in the streamwise velocity at $r = \pm D/2$ in Fig. 3 (right). As shown by Fig. 3 (left), the values of the velocity in front of the disk plane ($x = 0$) are further affected by the non-zero disk thickness. The radial evolution of the velocity deficit in the near-wake is however well represented numerically (Fig. 3 right).

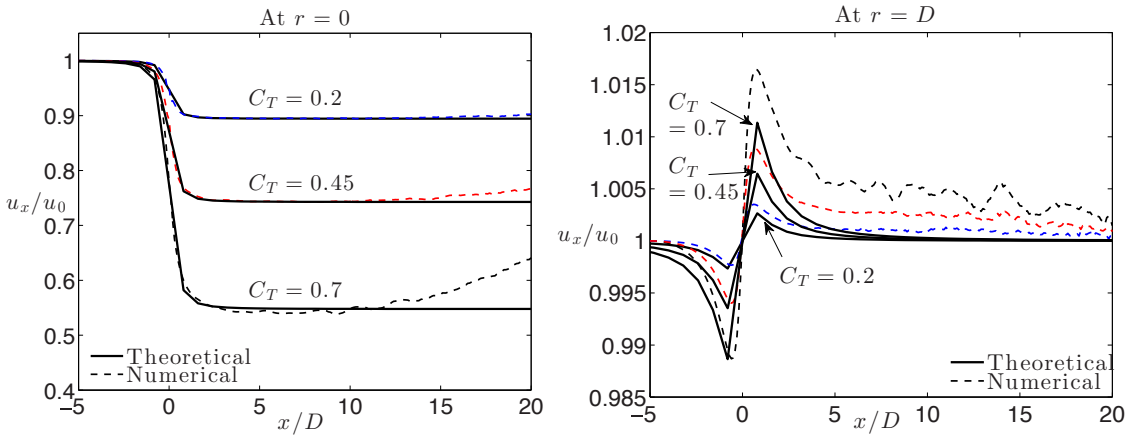

Figure 2: Streamwise evolution of the streamwise velocity (non-dimensionalised by the far-upstream velocity) at $r = 0$ (left) and $r = D$ (right), for an actuator-disk of diameter D centred at $x = 0$, and three values of thrust coefficient C_T. The lines represent the semi-analytical solution [8], while the dashed lines show the numerical results.

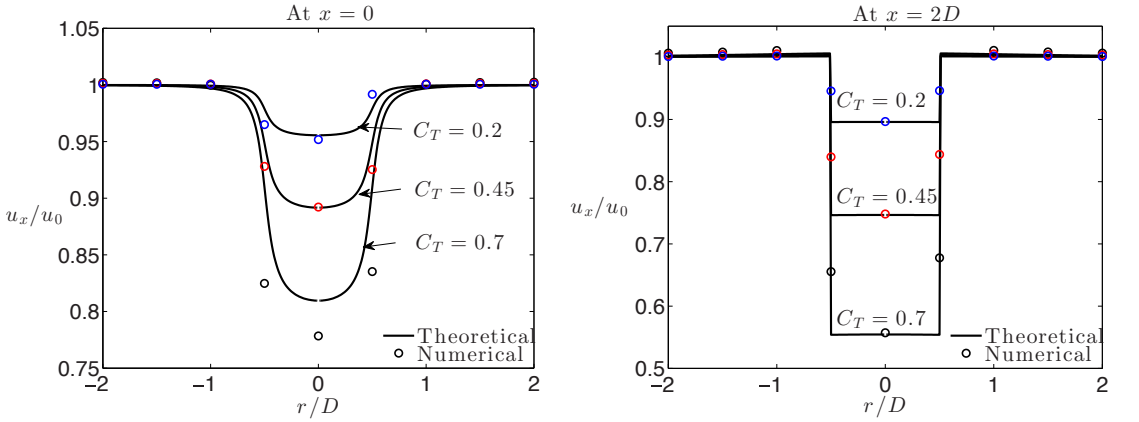

Figure 3: Radial evolution of the streamwise velocity (non-dimensionalised by the far-upstream velocity) at $x = 0$ (left) and $x = 2D$ (right), for an actuator-disk of diameter D centred at $x = 0$, and three values of thrust coefficient C_T. The lines represent the semi-analytical solution [8], while the symbols show the numerical results.

3.2. Dynamics of a floating pile

The dynamic response of a pile is analysed when placed at the interface between air ($\rho_1 = 1.2kg, \mu_1 = 18.27\mu Pa \cdot s$) and water ($\rho_2 = 1000kg, \mu_2 = 1.002mPa \cdot s$). The pile density is uniform and equals half the water density. The fluid phases are assumed to be immiscible. A volume-fraction field α_f, varying between 0 and 1, is associated with each fluid and they collectively sum to 1 across the domain. An advection-diffusion equation is solved for the volume-fraction fields, in order to track the air-water interface in time. A flux-limiting scheme replaces the need for interface reconstruction and particle tracking, hence simplifying the interface tracking method on unstructured meshes [27]. Consistent discretisations for the momentum and material advection steps further ensure conservation of α_f. The advection-diffusion equation is solved on a dual control-volume mesh, for a piecewise-constant

representation of the volume-fraction fields. The advective fluxes are limited using the HyperC approach [27], and the Bassi-Rebay discretisation scheme is used for the diffusion term [1]. In this work, the velocity field is further piecewise constant, while the pressure field varies linearly over the elements. The extension to higher-order finite-element pairs for velocity and pressure is the subject of future work. The pile is centred in a box of edge length $20D$, where D is the pile diameter and $4D$ is its length. The fluid mesh is adapted at every six time-steps and refines the regions of high curvatures in the solid-concentration and fluid-concentration fields. The mesh resolution is therefore increased at the fluid-solid and air-water interfaces. The total number of mesh elements is in the order of 10^5. The minimum and maximum values of the element-edge length are respectively of the order of $l_e/D = 0.015$ and $L_e/D = 0.8$. The time step varies throughout the run, in order to ensure that the Courant number equals 0.2. The simulation is ran on one CPU and requires approximately 15 hours of run time per second of physical time. Initially, the fluids are at rest and the pile lies vertically across the fluid interface (Fig. 4). Because the pile position is not stable, it starts moving in heave before falling into water. The pile eventually reaches an equilibrium position, which is horizontal and half submerged in water following Archimedes' principle. In the current simulations, the equilibrium position is reached after approximately 4 seconds of physical time although the pile continues to pitch slightly around the equilibrium position as time evolves. Although the present results agree with the expectations, on-going work focuses on more detailed comparisons for wave-structure interactions with a moving pile.

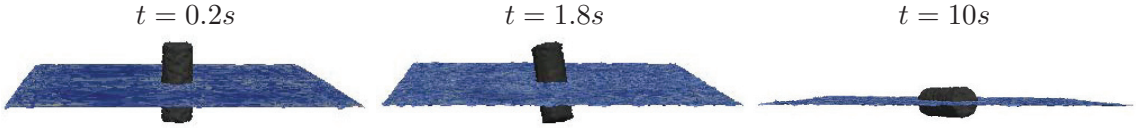

Figure 4: Snapshots of the dynamics of a floating pile, at three different instants in time, when placed at the interface between air and water.

4. Conclusions

This work applies a novel algorithm that couples two finite-element models on two cases for which semi-analytical solutions exist, i.e. (i) the flow past a fixed wind turbine represented by an actuator disk, and (ii) the dynamics of a cylindrical pile floating at the interface between air and water. The coupling between two separate models allows for specific numerical requirements to be met for each material. Thus, this work provides a versatile tool for modelling interactions between fluids and floating solids. Also, each model solves the full set of non-linear equations for the fluid- and solid- dynamics. The approach is novel in that spatial conservation is verified independently of the mesh resolution and the types of mesh used in both models. To the authors' knowledge, previous studies enabling spatial conservation are limited in terms of mesh shape at the fluid-solid interface (e.g. coinciding meshes in both models) and/or level of representation of the discrete fields. The results show that the present coupled models are able to: (i) accurately predict the velocity deficit induced by a fixed and uniformly-loaded actuator disk, and (ii) represent the balance of forces acting on a pile which floats at an air-water interface. Future work will build up towards the modelling of more complex turbine models and realistic floating wind turbine supports, with the objective to analyse the detailed dynamics of a single floating wind turbine over short time intervals.

Acknowledgements

This work is supported by the European Union Seventh Framework Programme (FP7/2007-2013) under a

Marie-Curie Intra-European Fellowship (grant agreement PIEF-GA-2010-272437). The authors also wish to acknowledge support from EPSRC, NERC, the Grantham Institute for Climate Change, and the High Performance Computing Service at Imperial College London. The content of this paper reflects only the author's views and not those of the European Commission.

References

[1] Bassi F and Rebay S, A high-order accurate discontinuous finite element method for the numerical solution of the compressible Navier-Stokes equations, *J Comput Phys* 1997; **131**:267–279.
[2] Calaf M, Parlange MB, Meneveau C, Large eddy simulation study of scalar transport in fully developed wind-turbine array boundary layers, *Phys. Fluids* 2011, **23**:126603.
[3] Castellani F, Vignaroli A, An application of the actuator disc model for wind turbine wakes calculations, *Applied Energy* 2013; **101**:432–440.
[4] Conway J, Analytical solutions for the actuator disk with variable radial distribution of load, *J Fluid Mech* 1995; **297**:327–355.
[5] Griffith BE, Hornung RD, McQueen DM, Peskin CS, An adaptive, formally second order accurate version of the immersed boundary method. *J Comput Phys* 2007; **223**:10–49.
[6] Jonkman J, Larsen T, Hansen A, Nygaard T, Maus K, Karimirad M, Gao Z, Moan T, Fylling I, Nichols J, Kohlmeier M, Pascual Vergara J, Merino D, Shi W, Park H, Offshore code comparison collaboration within IEA wind task 23: Phase IV Results regarding floating wind turbine modeling, *National Renewable Energy Laboratory* 2010; NREL/CP-500-47534:1–23.
[7] Karimirad M, Moan T, A simplified method for coupled analysis of floating offshore wind turbines, *Marine Structures* 2013; **27**: 45–63.
[8] Karimirad M, Modelling aspects of a floating wind turbine for coupled wave-wind-induced dynamics analyses, *Renewable Energy* 2013; **53**: 299–305.
[9] Madsen HA, Bak C, Døssing M, Mikkelsen R, Øye S, Validation and modification of the blade element momentum theory based on comparisons with actuator disc simulations, *Wind Energy* 2010; **13**: 373–389.
[10] Maguire AE, Hydrodynamics, control and numerical modelling of absorbing wavemakers, PhD thesis, The University of Edinburgh, 2011.
[11] Mark A, van Wachem BGM, Derivation and validation of a novel implicit second-order accurate immersed boundary method. *J Comput Phys* 2008; **227**:6660–6680.
[12] Mikkelsen R, Actuator disc methods applied to wind turbines, PhD thesis, Technical University of Denmark, 2003.
[13] Mittal R, Iaccarino G, Immersed boundary methods. *Annu Rev Fluid Mech* 2005; **37**:239–261.
[14] Pain C, Piggott M, Goddard A, Fang F, Gorman G, Marshall D, Eaton M, Power P, de Oliveira C, Three-dimensional unstructured mesh ocean modelling, *Ocean Modelling* 2005; **10**:5–33.
[15] Peskin CS, Flow patterns around heart valves: a numerical method. *J Comput Phys* 1972; **10**:252–271.
[16] Piggott MD, Gorman GJ, Pain CC, Allison PA, Candy AS, Martin BT, Wells MR, A new computational framework for multi-scale ocean modelling based on adapting unstructured meshes, *Int J Numer Meth Fluids* 2008; **56**:1003–1015.
[17] Réthoré P-E, Bechmann A, Sørensen NN, Frandsen ST, Mann J, Jørgensen HE, Rathmann O, Larsen SE, A CFD model of the wake of an offshore wind farm using a prescribed wake inflow, *J. Phys. Conf. Ser.* 2007, **75**:012047.
[18] Sebastian T, Lackner M, Characterization of the unsteady aerodynamics of offshore floating wind turbines, *Wind Energy* 2013; **16**: 339–352.
[19] Sebastian T, Lackner MA, Development of a free vortex method code for offshore floating wind turbines, *Renewable Energy* 2012; **46**: 269–275.
[20] Sethuraman L, Venugopal V, Hydrodynamic response of a stepped-spar floating wind turbine: numerical modelling and tank testing, *Renewable Energy* 2013; **52**: 160–174.
[21] Spinneken J, Heller V, Kramer S, Piggott M, Viré A, Assessment of an advanced finite element tool for the simulation of fully-nonlinear gravity water waves, *Int J Offshore and Polar Eng* 2012; **3**:1043–1050.
[22] Viré A, How to float a wind turbine. *Rev Environ Sci & Biotech* 2012; **11**:223–226.
[23] Viré A, Xiang J, Milthaler F, Farrell PE, Piggott MD, Latham JP, Pavlidis D, Pain CC, Modelling of fluid-solid interactions using an adaptive mesh fluid model coupled with a combined finite-discrete element model. *Ocean Dyn* 2012; **62**:1487–1501.
[24] Viré A, Xiang J, Piggott M, Spinneken J, Pain C, Numerical modelling of fluid-structure interactions for floating wind turbine foundations, *Proceedings of the 23rd International Ocean and Polar Engineering Conference* 2013; in press.
[25] Viré A, Xiang J, Piggott MD, Cotter CJ, Pain CC, Numerical modelling of fluid-structure interactions for floating actuator discs, *Proceedings of the International Conference on Aerodynamics of Offshore Wind Energy Systems and Wakes* 2013; in press.
[26] Xiang J, Munjiza A, Latham JP, Finite strain, finite rota- tion quadratic tetrahedral element for the combined finite-discrete element method. *Int J Numer Methods Eng* 2009; **79**:946–978.
[27] Wilson CR, Modelling multiple-material flows on adaptive, unstructured meshes, PhD thesis, Imperial College London, 2009.